東京大学　大学院新領域創成科学研究科
基盤科学研究系

先端エネルギー工学専攻

平成22年度
修士論文

Internal Structure and Precursor of Laser Supported Detonation - レーザー支持爆轟波のプリカーサーと内部構造-

2011年2月提出
指導教員　小紫　公也　教授

96070　嶋村　耕平

PREFACE

The present paper is concerned with laser-supported detonation(LSD) that have been investigated intensively in the last decade and represent a possibility of application for laser propulsion. The laser wavelength dependency on LSD wave is discussed in the first part of the paper. A development of high power Neodymium glass (Nd:glass) laser makes a application possibility on laser propulsion. The Nd:glass laser is one of a candidate of the driver for the propulsion. Previous study found that plasma induced using the glass laser absorbed the laser energy during short LSD regime as compared with CO_2 laser. Beside, laser absorption efficiency for glass laser is much higher than that for CO_2 laser. To investigate a influence of laser wavelength for LSD wave in comparison with the CO_2 laser, we used plasma emission spectroscopy and measured the electron temperature and electron density. Furthermore, we estimated a laser absorption layer, which is based on the equation of inverse bremsstrahlung absorption.

The second part is concerned with photoionization ahead of shock wave induced by UV radiation. Precursor electrons ahead of a shock wave have been recognized as certain role, like absorbing the laser energy, for sustaining the LSD wave. Photoionization by Ultraviolet (UV) radiation behind the shock wave generate the electrons. To evaluate UV photons emission from plasma, we measured a number density of electrons and the electron temperature and estimated the absorption layer and the radiation volume. And high-purity argon was used as the test gas for comparison with air. Argon gas is one of the inert gases and its ionization and excitation processes are simple comparing with air.

The author would like to thank Professor Kimiya Komurasaki, who helped to find this avenue of research to begin with, and also was of great assistance in developing this experiment and document. I would also like to express my sincere thanks to Professor Yoshihiro Arakawa, who told me how an engineer and a researcher should be. I received many helps from Dr. Yasuhisa Oda in the Japan Atomic Energy Agency and Dr. Shigeru Yokota in the University of Nagoya. For research assistance, thanks to: Bin Wang, Keisuke Michigami, Taro Han, Toshikazu Yamaguchi, Yutaka Shimada, Reiji Komatsu, Tony Schoenherr, Masafumi Fukunari and Akinori Oda. Finaly, this work is supported by a Grant-in-Aid for Scientific Research (a), No. 19296987, sponsored by the Ministry of Education, Culture, Sports, Science and Technology, Japan.

KOHEI SHIMAMURA
February 2011

Contents

1 INTRODUCTION **1**

2 LASER WAVELENGTH DEPENDENCY ON LASER SUPPORTED DETONATION **4**

2.1 Introduction 4
2.2 Experimental Setup 5
2.2.1 Laser and focusing optics 5
2.2.2 Emission Spectroscopy 7
2.3 Electron Temperature and Electron Density 8
2.4 Structure of Laser Absorption Process in LSD Wave 10
2.5 Conclusion 13

3 PHOTOIONIZATION IN PRECURSOR OF LASER SUPPORTED DETONATION BY ULTRAVIORET RADIATION **16**

3.1 Introduction 16
3.2 Laser Shadowgraphs 17
3.3 Electron Temperature and Electron Density 19
3.4 Radiation Volume 20
3.5 Photon Emission Rate 22
3.6 Conclusion 22

4 CONCLUSION **25**

List of Figures

2.1 Development of high power glass laser for fusion device[10]."Line+scatter" is a respectively pulse laser(right originate axis). 6
2.2 Temporal change of the displacements of the shock wave and the ionization wave (focus number: 6.3, ambient pressure: 101.3 kPa) for a Nd:glass laser[17] and the laser pulse shape (1 J/pulse). 7
2.3 Temporal change of the displacements of the shock wave and the ionization wave (focus number: 2.2, ambient pressure: 101.3 kPa) for a CO_2 laser[13] and the laser pulse shape (10 J/pulse). 7
2.4 Schematic of the emission spectroscopy system. 8
2.5 Boltzmann plot of NII at t = 0.3 - 0.5 μs. 9
2.6 Stark Broadening of NII 399.5 nm at t = 0.3 - 0.5 μs. 9
2.7 Electron temperature and electron density with using the glass laser. 10
2.8 Electron temperature and electron density with using the CO_2 laser[19]. 10
2.9 Laser power density on the LSD wave front S for the Nd:glass laser and the CO_2 laser. 11
2.10 Absorption layer length l_a and number density of neutral particle of Nd:glass Laser. 11
2.11 Absorption layer length l_a and number density of neutral particle of TEA CO_2 Laser[19]. 12

3.1 Model of UV radiation from LSD wave. 17
3.2 Schematic of laser shadow graph experiment. 18
3.3 Argon laser plasma at t = 3.4 μs. 18
3.4 Laser pulse shape, displacement of the shock front and the ionization front, and Mach-number as compared with air plasma[6]. 19
3.5 Boltzmann plot of ArI at t = 0.3 μs. 20
3.6 Stark Broadening of ArI at t = 0.3 μs. 20
3.7 Electron temperature and electron density for argon plasma as compared with air plasma. 21
3.8 Schematic and approximation model for the LSD wave. 21
3.9 Photon emission rate and absorption layer length for air and argon atmosphere. 22

Chapter 1

INTRODUCTION

Air-breathing laser propulsion is a candidate for a low cost lauching.[1] It can be considered as a mass driver, in which a vehicle is acclerated by the laser power transmitted remotely from the ground. Since this propulsion does not consume fuel on board, it is more advantageous than a conventional rocket. These advantages make the lower cost lauching, which is 100 times than that of conventional rocket.

Detonation waves induced using a pulse laser are attracting great interest for use in air-breathing laser propulsion. Understanding important aspects of the internal structure of the laser-supported detonation wave is important for designing vehicles. In laser-supported detonation (LSD), a laser absorption layer propagating with the shock wave corresponds to a combustion layer in chemical detonation.[2] The gas used in LSD is heated at almost constant volume, at which the kinetic energy transfers the laser energy efficiently. Because the laser intensity decreases to a threshold, the shock wave front and the ionization front separate and the LSD terminates. Then energy conversion from laser energy to kinetic energy stops. Thereafter, the shock wave propagates adiabatically.

Raizer specifically examined the energy balance between the energy input via laser heating and the energy loss from the LSD region to a surrounding blast wave and reported that the LSD terminates when the ratio of the laser absorption layer thickness to the diameter of the laser-beam cross section exceeds a threshold.[3] Earlier reports of the literature describe dependencies of the LSD wave characteristics on the focused number of laser beams, the laser pulse energy, and ambient air pressure. In addition, using a CO_2 laser in air, Mori studied the blast-wave energy efficiency and the laser power-density threshold for LSD termination.[4] Ushio investigated features of a line-focused-laser inducing the LSD wave in quasi-1D space and 2D to restrict an enthalpy spill from the LSD wave.[5] His results showed that the lateral enthalpy spill is a key factor for the condition of LSD termination. However, its mechanism was explained without consideration of the radiation and ionization phenomena in an LSD wave. From the view of gas discharge physics, the precursor electrons ahead of the shock wave play an important and defined role, such as absorbing the laser energy, for sustaining the LSD wave.[6]

The present paper is concerned with laser-supported detonation(LSD) that have been investigated intensively in the last decade and represent a possibility of

application for laser propulsion. The laser wavelength dependency on LSD wave is discussed in the first part of the paper. A development of high power Neodymium glass (Nd:glass) laser makes a application possibility on laser propulsion. The Nd:glass laser is one of a candidate of the driver for the propulsion. Previous study found that plasma induced using the glass laser absorbed the laser energy during short LSD regime as compared with CO_2 laser. Beside, laser absorption efficiency for glass laser is much higher than that for CO_2 laser. To investigate a influence of laser wavelength for LSD wave in comparison with the CO_2 laser, we used plasma emission spectroscopy and measured the electron temperature and electron density. Furthermore, we estimated a laser absorption layer, which is based on the equation of inverse bremsstrahlung absorption.

The second part is concerned with photoionization ahead of shock wave induced by UV radiation. Precursor electrons ahead of a shock wave have been recognized as certain role, like absorbing the laser energy, for sustaining the LSD wave. Photoionization by Ultraviolet (UV) radiation behind the shock wave generate the electrons. To evaluate UV photons emission from plasma, we measured a number density of electrons and the electron temperature and estimated the absorption layer and the radiation volume. And high-purity argon was used as the test gas for comparison with air. Argon gas is one of the inert gases and its ionization and excitation processes are simple comparing with air.

Bibliography

1) H. Katsurayama, K. Komurasaki, and Y. Arakawa, Acta Astronautica 65, 1032 (2009).

2) F. A. Williams, Combustion Theory; 2nd edition, Westview Press, Boulder, 1994.

3) Y.P. Raizer, Laser-Induced Discharge Phenomena, Studies in Soviet Science (Consultant Bureau, New York, 1977).

4) K. Mori, K. Komurasaki, and Y. Arakawa, J. Appl. Phys. 92, 5663 (2002).

5) M. Ushio, K. Kawamura, K. Komurasaki, and Y. Arakawa, Shockwaves 18(1), 35 (2008).

6) Raizer, Y. P., Gas Discharge Physics, Springer, Berlin, 1991.

Chapter 2

LASER WAVELENGTH DEPENDENCY ON LASER SUPPORTED DETONATION

2.1 Introduction

A possibility of using high power lasers for the space propulsion system was proposed soon after the invention of the laser[1]. From 70 's through the present, many researchers investigated the laser propulsion using the many types of craft and the high power lasers[2–4]. Myrabo et al. investigated the flight demonstrations using a 10-kW-class repetitive pulse CO_2 laser. Their demonstrations were set with a flight lasting 11 seconds and reaching 72 m[5]. Sasoh et al. also studied the laser propulsion, which is called as Laser In-Tube Accelerator (LITA), experimentally using a 6-J pulse CO_2 laser[6]. In this way, several high power CO_2 lasers were being used for these experiments and much more. On the one hand, the CO_2 laser is, apparently, one of the earliest gas lasers and the most useful, whose laser pulse energy has become up to 1 kJ, has been realized today[7,8]. On the other hand, recently, the development of high power glass Neodymium glass (Nd:glass) laser makes the application possibility for the laser propulsion. Nd:glass laser is one of the solid state laser that uses a gain medium, which is a solid, rather than a liquid or a gas and has been designed and used for the purpose of conducting laser fusion researches[8]. The peak power of Nd:glass laser is up to 10^3 TW[9] , and market share of high power glass laser increase more and more than TEA CO_2 laser[10]. To these consideration, Nd:glass laser is one of the candidate of the driver for the laser propulsion and should be compared the specifications of ability for laser propulsion with CO_2 laser.

Furthermore, understanding the mechanism of laser plasma might help for the development of laser propulsion. In terms of application for laser propulsion, Laser Supported Detonation (LSD) is the one of most important phenomena. In the LSD, a laser absorption layer propagating with the shock wave corresponds to a combustion layer in chemical detonation[11,12]. The gas used in LSD is heated almost at constant volume where the kinetic energy transfers the laser energy

efficiently. As the laser intensity decreases to a threshold, the shock wave front and the ionization front separate and the LSD terminates, after which energy conversion from laser energy to kinetic energy much decreases. Then the shock wave propagates adiabatically. Thus, the process of energy conversion strongly influences the termination of LSD.

In our previous study, the characteristic of the laser induced plasma were investigated, such as laser power density on LSD S, the LSD termination and the energy conversion efficiency η_{bw}, which were mainly investigated by a TEA CO_2 laser[13–16]. The performance of the laser propulsion is usually evaluated with the momentum coupling coefficient C_{m} that is a function of ${\eta_{\mathrm{bw}}}^4$. Thus, η_{bw} is a one of the performance parameter for the respectively pulse laser propulsion. Wang et al. investigate these parameters using Nd:glass laser and compared the results with the previous study[17]. The results show that the blast wave energy efficiency in these lasers is almost same order at 40%. Furthermore, the LSD duration in TEA CO_2 laser and Nd:glass laser are about 1.3 μs and 0.3 μs, respectively.

What makes the difference for η_{bw} and the LSD regime termination between the Nd:glass laser and CO_2 laser? Despite the blast wave induced with the Nd:glass laser can absorb the laser energy as almost same order, the LSD regime that is the main absorption process for the glass laser appears to have even low value than that for the CO_2 laser. The present study explores experimentally the characteristics of laser plasma, such as the electron temperature and electron density, using Nd:glass laser and compares the absorption coefficients[18] $k_{\mathrm{e-i}}$ and $k_{\mathrm{e-n}}$ with these lasers. Furthermore, these results were discussed from the point of view of the laser absorption process. The present study explores experimentally the characteristics of laser plasma using a spectroscopic study. The electron temperature was estimated using Boltzmann method and the electron temperature was evaluated using the Voigt function fitting. Then, the photon means free path can be estimated with using the temperature and density. Finally, we discussed the structure of laser absorption in terms of laser wavelengths.

2.2 Experimental Setup

2.2.1 Laser and focusing optics

A Nd:glass laser produces a pulse of 33 ns pulse width (FWHM) at 1,053 nm for all conditions; about 62 % of all pulse energy is irradiated in 66 ns (double the FWHM pulse width), which was used in our previous study[17]. Temporal laser power profiles obtained using the photo detector (ET-2000; Electro Optics Technology, Inc.) are presented in Fig.2.2. Its single pulse energy is up to 2 J, with a circle cross section area of 10 mm diameter. The laser pulse consisted of a leading spike and a following exponentially decaying tail lasting around 900 ns. Temporal variations of the shock front and plasma front displacements on the beam axis are also shown in Fig.2.2[17]. To generate the breakdown spark, the lens with 62.7 mm focal length focused the laser beam without any target. Besides, a TEA CO2 pulse laser was used, as in our previous studies[4,13–16]. Its pulse shape measured

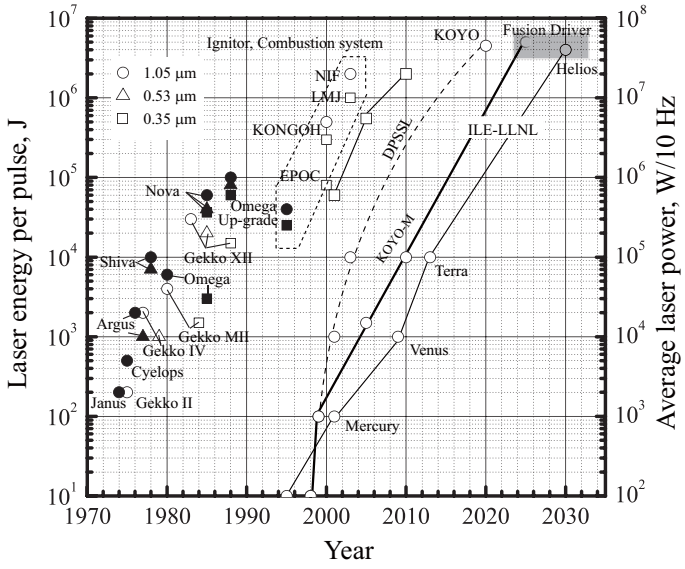

Figure 2.1: Development of high power glass laser for fusion device[10]."Line+scatter" is a respectively pulse laser(right originate axis).

Table 2.1: Spectral line data for NII from NIST[7].

	λ (nm)	A_{ik} (10^7 s^{-1})	E_k (eV)	g_k
N II	391.900	6.76	23.57	3
	395.585	1.31	22.00	5
	399.500	13.5	22.00	5
	444.703	11.4	23.20	5
	504.510	3.42	20.94	3

by a photo detector (B749; Hamamatsu photonics, Inc.) is shown in Fig.2.3. The pulse is composed of a leading edge spike and a following exponentially decaying tail. The FWHM of the spike was 120 $\pm$ 20 ns. The tail decay constant was 1.15 $\pm$ 0.05 μs. Its single pulse energy is 10 J, with a square cross section area of 30 mm $\times$ 30 mm (The transverse mode is Gaussian in the vertical direction and top-hat shape in the horizontal direction). The pulse energy was measured before and after the experiments using a joule meter; subsequent shot-to-shot the pulse energy fluctuations were kept below 5 % throughout experimentation. Temporal variations of the shock front and plasma front displacements on the beam axis are also shown in Fig.2.3[14]. The incident laser beam is first reflected and line-forced using a 2-D parabolic mirror[16].

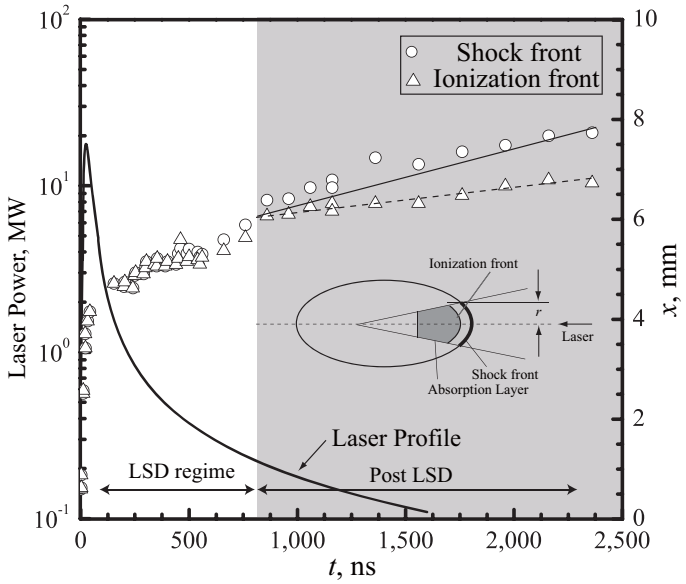

Figure 2.2: Temporal change of the displacements of the shock wave and the ionization wave (focus number: 6.3, ambient pressure: 101.3 kPa) for a Nd:glass laser[17] and the laser pulse shape (1 J/pulse).

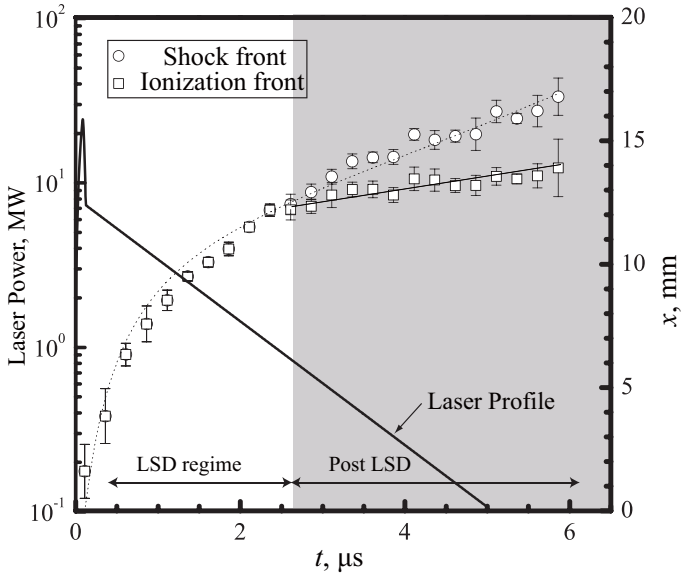

Figure 2.3: Temporal change of the displacements of the shock wave and the ionization wave (focus number: 2.2, ambient pressure: 101.3 kPa) for a CO_2 laser[13] and the laser pulse shape (10 J/pulse).

2.2.2 Emission Spectroscopy

The emission spectroscopy measurement for the glass laser experiment is carried out to investigate the diagnostics of the laser induced plasma. Figure 2.4 portrays

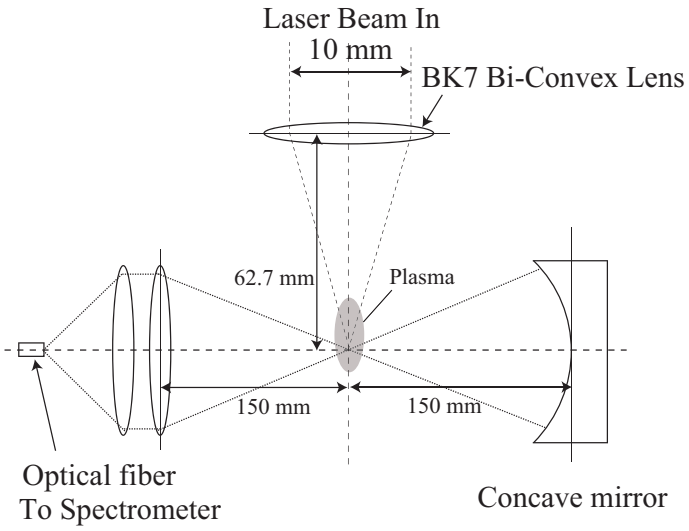

Figure 2.4: Schematic of the emission spectroscopy system.

a schematic of the emission spectroscopy experiment. The irradiance of the plasma is collected using the lenses and the optical fiber and analyzed using an Echelle spectrometer (Aryelle200; Lasertechnik Berlin Inc.) with spectral resolution $\lambda/\Delta\lambda$ is 8,000, which is in the range of wavelength 250-900 nm. Each spectral line was taken with an ICCD camera (iStar 734-18-F-03; Andor Technology Inc.) that has the resolution intensifiers of 1,024 $\times$ 1,024 pixels and the minimum exposure time of 5 ns. The time integrated intensifiers were 100 ns for all of data using CO_2 laser and 30($<$ 600 ns)-100 ns using Nd:glass laser. Calibration of wavelength was done using a Hg-lamp in the spectrometer and the calibration of sensitivity was done using a halogen lamp. It was just one taken with a series of experiments where the time was adjusted. Note that no spatial information of the spark was resolved.

2.3 Electron Temperature and Electron Density

An information of T_e can be inferred using the Boltzmann plot method with assuming the local thermal equilibrium that can be expressed as shown below[19].

$$\ln \frac{\varepsilon_{ik} \lambda_{ik}}{A_{ik} g_k} = -\frac{E_k}{k_B T_{ex}} + \ln K \tag{2.1}$$

where $A_{ik}, E_k, \varepsilon_{ik}, g_k, \lambda_{ik}, k_B$ and K represent the transition probability, the upper level energy, the emission coefficient of the spectral line, the upper statistical weight, the wavelength of the line, the Boltzmann 's constant and the constant, respectively. Figure 2.5 presents an example of applying this method at the time of $t = 0.3$ μs and shows that each data plot appears on the line. This results indicate that the electrons in the plasma layer are in the local thermal equilibrium.

In order to estimate n_e, the stark broadened profile was used. This method has the assumption that the stark effect dominantly generates the line broadening, in

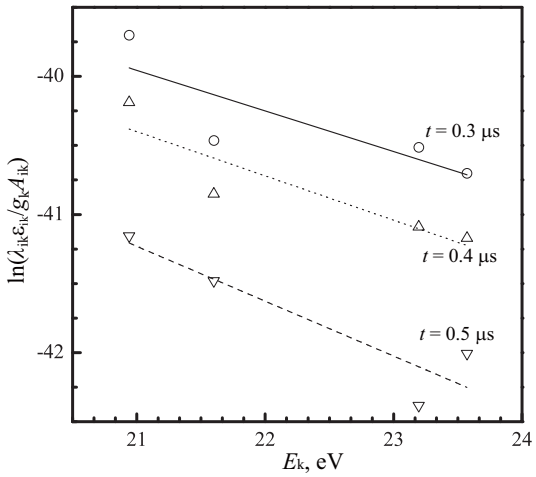

Figure 2.5: Boltzmann plot of NII at t = 0.3 - 0.5 μs.

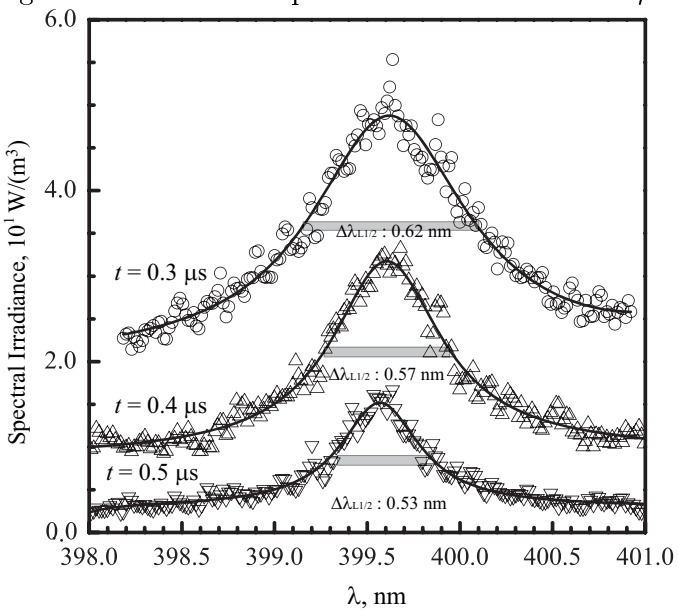

Figure 2.6: Stark Broadening of NII 399.5 nm at t = 0.3 - 0.5 μs.

comparison with the other broadening mechanisms. The spectral lines were fitted with the Voigt function, which was deconvolution model for Lorentzian function and Gauss function. For the laser plasma, the pressure broadening is negligible, in comparison with the stark broadening[8]. Thus, the stark effect is the dominant broadening in the Lorentzian function. The full width of half maximum of a Stark broadening $\Delta\lambda_{\mathrm{stark}}$ (nm) is a function of n_{e} and the electron-impact half width W, which was obtained from Griem[19], that can be expressed as[8],

$$\Delta\lambda_{\mathrm{stark}} = 2W\frac{n_{\mathrm{e}}}{10^{17}} \tag{2.2}$$

The measurements of electron density were deduced from the N^+ five-lines. Figure

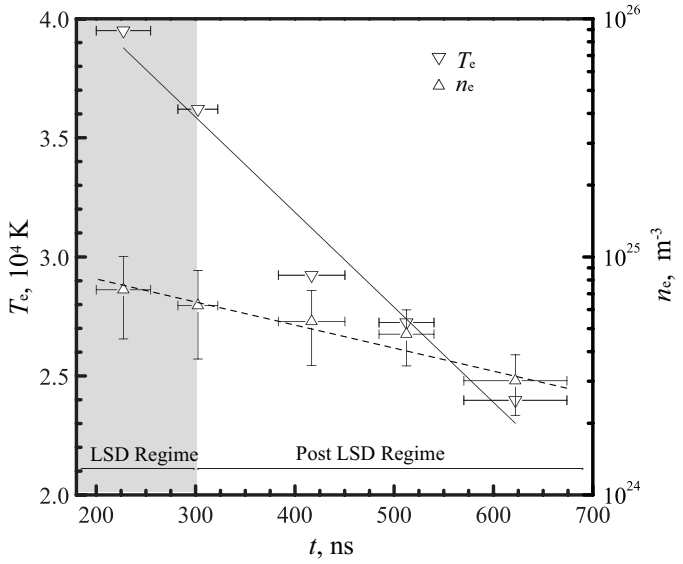

Figure 2.7: Electron temperature and electron density with using the glass laser.

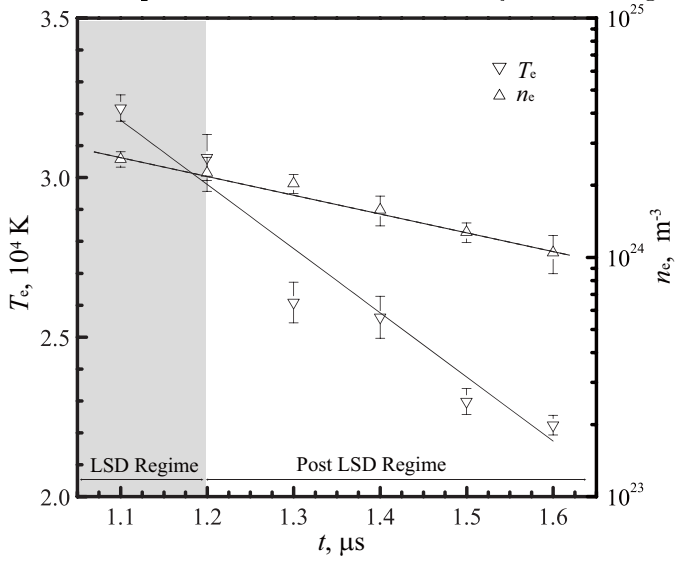

Figure 2.8: Electron temperature and electron density with using the CO_2 laser[19].

2.6 shows one of the result applying this method at $t = 0.3$ μs. The temporal evolution of ne and Te are shown as Fig.2.7 and Fig.2.8, respectively. For both of T_e and n_e, each data plot for the glass laser appears to have even low value than for CO_2 laser.

2.4 Structure of Laser Absorption Process in LSD Wave

In Raizer 's model, termination of the LSD depends on the magnitude of the plasma layer l behind the shock wave and the laser beam radius r at the shock

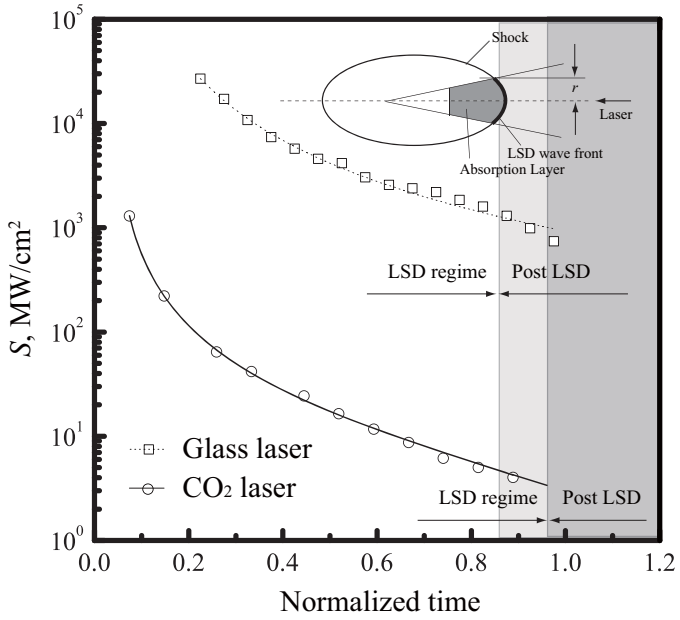

Figure 2.9: Laser power density on the LSD wave front S for the Nd:glass laser and the CO_2 laser.

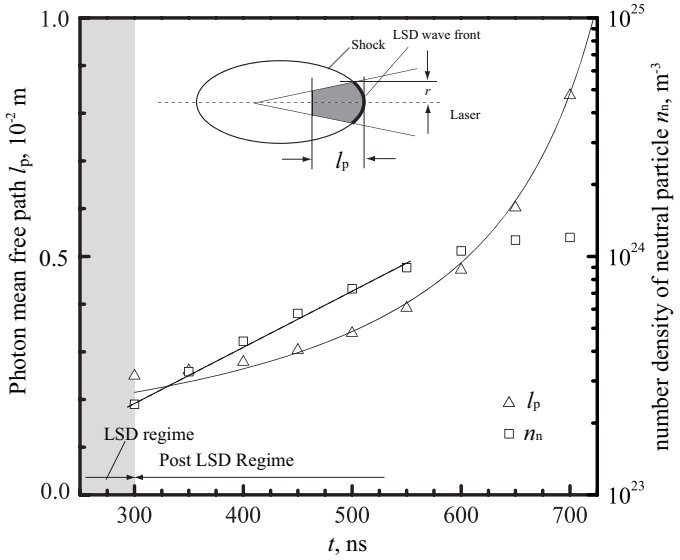

Figure 2.10: Absorption layer length l_a and number density of neutral particle of Nd:glass Laser.

front. It is defined that the LSD termination would occure when the plasma length approaches 4 r as[11],

$$l_{\text{term}} = 4r_{\text{term}} \tag{2.3}$$

where, subscript term is values at the termination. Following this theory, in present study, the laser beam radius in the glass laser is 1/20 less than in the CO_2 laser.

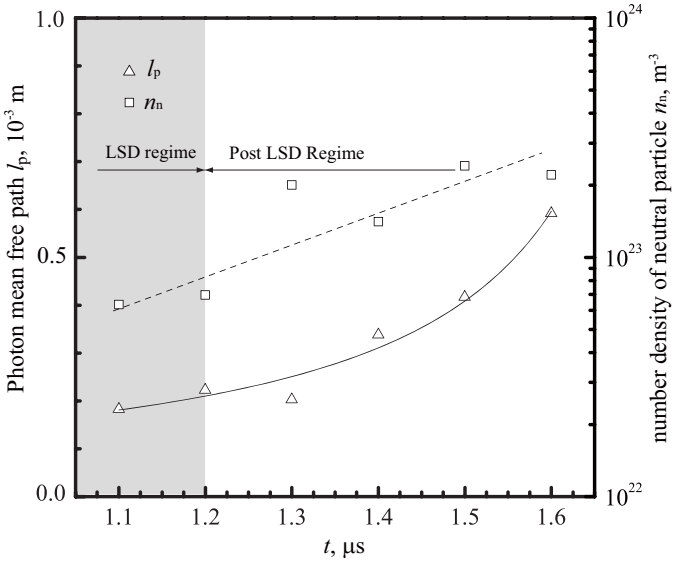

Figure 2.11: Absorption layer length l_a and number density of neutral particle of TEA CO_2 Laser[19].

Thus, the laser absorption layer and the laser absorption coefficient in the glass laser respectively were estimated approximately at 1/20 and 20 times as much as in the CO_2 laser. However, laser beam of intensity I is mainly absorbed in the process of inverse Bremsstrahlung that involves the interaction of electrons and with either ions or neutrals particles[11]. This absorption process is described by an absorption coefficient k_L defined as,

$$\frac{dI}{dx} = -k_L I = -(k_{e-i} + k_{e-n})I \tag{2.4}$$

Therein, k_{e-i} and k_{e-n} respectively stand for the energy transfer between the electron and ion and between the electron and neutral particles. These coefficients can be expressed as Eqs. (2.5) and (2.6) and the laser absorption layer l_a (= 1/ (k_{e-i} + k_{e-n})) is defined as the reciprocal of this coefficients[18].

$$k_{e-i} = \frac{4}{3}\left(\frac{2\pi}{3m_e k_B T_e}\right)^{\frac{1}{2}} \frac{e^6\lambda^3}{hc^4 m_e} G n_e n_i \left(\exp\left(\frac{hc}{\lambda k_B T_e}\right) - 1\right) \tag{2.5}$$

$$k_{e-n} = \frac{k_B T_e^2 A(T_e)\lambda^3}{hc} n_e n_n \left(1 - \exp\left(-\frac{hc}{\lambda k_B T_e}\right)\right) \tag{2.6}$$

Here, G denotes the Gaunt factor, λ is the wavelength of laser, n_e, n_i and n_n are the number densities of electron, ion and neutral particles, T_e is the electron temperature, h signifies Planck 's constant, m_e is the electron mass, c stands for the speed of light, k_B represents the Boltzmann 's constant and $A(T_e)$ represents a parameter that can be referred from the literature[18]. n_n can be estimated with using the Saha ionization equation. The equation for a main ionization reaction in the thermal equilibrium plasma ($N \leftrightarrow N^+ + e^-$) is introduced here, which represents

the degree of ionization of that plasma.

$$\frac{n_{\mathrm{i}} n_{\mathrm{e}}}{n_{\mathrm{n}} + n_{\mathrm{e}}} = 2.419 \times 10^{21} T_{\mathrm{e}}^{\frac{3}{2}} \exp\left(-\frac{E_{\mathrm{k}}}{k_{\mathrm{B}} T_{\mathrm{e}}}\right). \tag{2.7}$$

Because $k_{\mathrm{e-i}}$ and $k_{\mathrm{e-n}}$ respectively are proportional to λ^3, it seems that the laser absorption layer in the glass laser is shorter than in the CO_2 laser. In fact quite the contrary happened, accordingly, these facts implied that the plasma at high temperature and density remains behind the shock wave in glass laser, which is might derived from the multiple ionization.

Since both of absorption coefficients $k_{\mathrm{e-i}}, k_{\mathrm{e-n}}$ are a function of n_{e}^2, the increasing number density of electrons influences the decreasing length of absorption layer. Accordingly, the laser power density irradiated on the LSD wave S also influences l_{a} due to increased n_{e} and can be expressed as[13]

$$S = \frac{P(t)}{\pi r^2} = \frac{4Pf^2}{\pi r^2}, \tag{2.8}$$

where P is the laser power and f stands for the focus number. The measured threshold for the regime transition S_{term} and the temporal changes S are shown in Fig. 2.9. For both glass laser and CO_2 laser, S decreased as time goes by. S_{term} for glass laser is 1.1×10^3 MW/cm^2, while that of CO_2 laser is 3.7 MW/cm^2, an increase of three orders of magnitude. Mori investigated that S_{term} was estimated at $3 - 7$ MW/cm^2 for the several focusing number using the CO_2 laser[13]. In fact quite the contrary happened, and then the elucidation of the LSD termination condition is impossible to solely the laser intensity.

Figure 2.10 and 2.11 portray l_{a} in the LSD wave and n_{n} for both of these laser experiments. Results reveal that each data l_{a} plot in the glass laser appears to have even low value than in CO_2 laser. This makes sense because the inverse Bremsstrahlung process depends on the electron density, and these parameters for the glass laser data were slightly higher than that for the CO_2 data. Consequently, the LSD wave induced using the glass laser is sustained with the highly dense plasma, in comparison with that using the CO_2 laser.

2.5 Conclusion

1,053 nm irradiation from a Neodymium glass laser and 10.6 μm irradiation from a transversely excited atmospheric CO_2 laser were focused. Characteristics of the LSD wave for the glass laser experiment, such as n_{e} and T_{e}, are investigated using the emission spectroscopy. Results reveal that n_{e} and T_{e} for the glass laser experiment appears to have even high value than that for CO_2 laser. Besides, the absorption layer for the glass laser is longer than that for the CO_2 laser. This is because the laser energy is mainly absorbed in the inverse Bremsstrahlung process that involves the interaction the electrons with either ions or neutrals. The absorption coefficients are a function of the laser wavelength λ and electron density n_{e}. Thus, the LSD wave induced using the glass laser is sustained with the highly dense plasma, in comparison with that using the CO_2 laser.

Bibliography

1) A. Kantrowitz, Aeronaut. Astronaut. 10, 74 (1972).

2) V. P. Ageev, A. I. Barchukov, F. V. Bunkin, V. I. Konov, V. P. Korobeinikov, B. V. Putjatin, and V. M. Hudjakov, Acta Astronautica 7, 79 (1980).

3) A. N. Pirri, M. J. Monsler, and Nebolsin.Pe, AIAA Journal 12, 1254 (1974).

4) K. Mori, K. Komurasaki, and Y. Arakawa, J. Spacecr. Rockets 41, 887 (2004).

5) L. M. Myrabo, D. G. Messitt, and F. B. Mead, Jr., AIAA Paper, 98-1001 (1998).

6) A. Sasoh, Journal De Physique Iv 10, 41 (2000).

7) K. Yasuoka, A. Ishii, T. Tamagawa, and I. Ohshima, Proceedings of SPIE, 1412, 32 (1991).

8) G. Bekefi, Principles of Laser Plasmas, Willey-Interscience, New York, 1977.

9) M. Satoh, Laser Handbook, Ohm-sha, Tokyo, Japan, 2005(in Japanese).

10) S. Nakai, Power Laser Technology, Ohm-sha, Tokyo, Japan, 1999(in Japanese).

11) Y.P. Raizer, Laser-Induced Discharge Phenomena, Studies in Soviet Science (Consultant Bureau, New York, 1977).

12) F. A. Williams, Combustion Theory; 2nd edition, Westview Press, Boulder, 1994.

13) K. Mori, K. Komurasaki, and Y. Arakawa, J. Appl. Phys. 92, 5663 (2002).

14) K. Mori, K. Komurasaki, and Y. Arakawa, J. Appl. Phys. 95, 5979 (2004).

15) K. Mori, K. Komurasaki, and Y. Arakawa, Appl. Phys. Lett. 88, 121502 (2006).

16) M. Ushio, K. Kawamura, K. Komurasaki, and Y. Arakawa, Shockwaves 18(1), 35 (2008).

17) B. Wang, K. Komurasaki, T. Yamaguchi, K. Shimamura, and Y. Arakawa, J. Appl. Phys. 108, 124911 (2010).

18) N. H. Kemp, and P. F. Lewis, Laser-heated thruster, NASA CR - 161665, 1980.

19) 嶋村 耕平, 畑井 啓吾, 河村 好一, 福井 章泰, 福田 章雄, 王 彬, 山口 敏和, 小紫 公也, 荒川 義博：2 波長マッハツェンダー干渉法を用いたレーザー支持爆轟波構造の解明, 日本航空宇宙学会論文集, 58, 323-329 (2010)

20) H. R. Griem, Plasma Spectroscopy, McGraw-Hill, New York, 1964.

Chapter 3

PHOTOIONIZATION IN PRECURSOR OF LASER SUPPORTED DETONATION BY ULTRAVIORET RADIATION

3.1 Introduction

Laser induced plasma and resulting strong shock wave have been attracting interests for laser propulsion[1–3]. In the initial stage of the plasma, a laser absorption layer propagates with the shock wave that corresponds to a combustion layer in chemical detonation. The structure has been recognized as a Laser Supported Detonation (LSD) wave. In terms of application for the propulsion, understanding important aspects of the internal structure of the wave is important for designing

A previous study shows that a precursor electron ahead of a shock wave has been investigated until LSD termination with using a two wave Mach-Zehnder interferometer[4]. Results of this study demonstrate that the laser heat sustained the LSD wave. Since laser heating induces the shock wave in the LSD, the LSD is difficult to sustain in separating the front of shock wave from the laser heating layer. The result suggests that the generation of the precursor electrons produces the preheated layer ahead of the shock wave. In other words, the precursor electrons play an important role in shock wave propagation. Furthermore, the phenomena is well known when dealing with a streamer and a sprite structures[5]. Photoionization ahead of ionized gas is due to photons emitted by atoms or molecular. These particles are transitted from excited state to a higher excited one. In air, molecular nitrogen with $N_2(C^3\Pi_u)$ state excited the UV radiation. The emission of this state is in a wavelength range 98.0 - 102.5 nm. Since molecular oxygen has a wavelength 102.5 nm corresponding ionization threshold, the molecular mainly absorbs due to photoionization in this range.

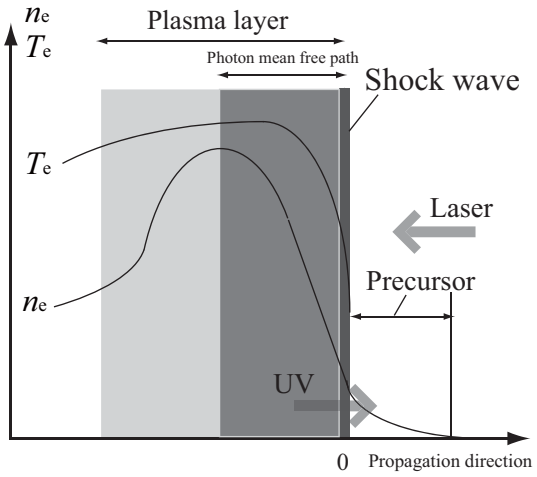

Figure 3.1: Model of UV radiation from LSD wave.

In this study, the propagation of shock wave and maintenance of LSD by laser energy are observed under the different ambient gases. A high-purity argon was used as the test gas for comparison with air. Argon gas is one of the inert gases and its ionization and excitation processes are simple comparing with air . To evaluate UV photons emission from plasma, we measured a number density of electrons and the electron temperature and estimated the absorption layer and the radiation volume. The plasma diagnostics was investigated with using the emission spectroscopy. In the following section, we measured the displacement of shock wave and ionization wave for both of the ambient gases. In this measurement, we investigated, quantitively, the influence of the gas species for the propagation of LSD. In Sec. 2.3, the electron temperature and the electron density were estimated for both cases. In Sec. 2.4, the laser absorption layer was estimated, which is based on the equation of inverse bremsstrahlung absorption. Then, we used an approximation model for laser plasma. Finally, we estimated the photons-contributing photoionization with using equation of the bremsstrahlung radiation.

3.2 Laser Shadowgraphs

Figure 3.2 shows the setup of the Schlieren graph method. A Nd:Glass laser used in the present study is the same as it in the former study[6]. The laser produces a pulse of 33 ns pulse width at 1,053 nm. Temporal laser power profiles obtained using a photodetector and the details terms of this laser are presented in the Fig.3.3. A beam of 40 mm in diameter was focused by a 150 mm focusing length lens and a beam expander outside a vacuum chamber. The chamber was filled with argon gas at 101.3 kPa after evacuation by a rotary vacuum pump. A YAG laser (CW, 532 nm, 1.0 W) was used as probe light. It projects the pictures of plasma on a high-speed ICCD camera (Ultra 8; DRS Technology Inc.) that enables us to take 8 frames in each laser pulse at a framing rate up to 100 million fps with the

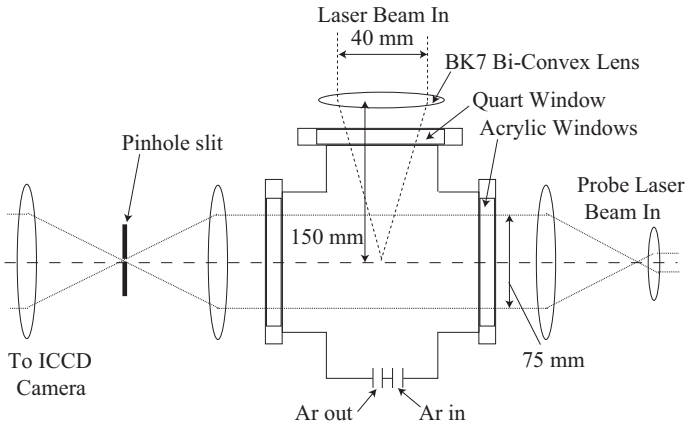

Figure 3.2: Schematic of laser shadow graph experiment.

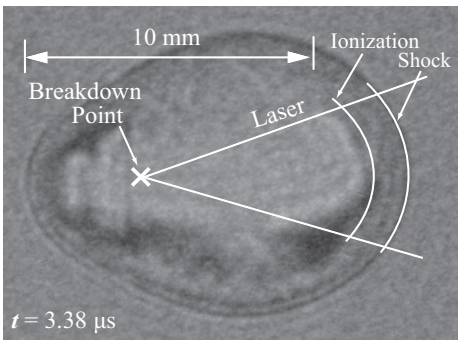

Figure 3.3: Argon laser plasma at $t = 3.4$ μs.

minimum exposure time of 10 ns. The synchronization between the ignition and the photographing is mainly controlled by a delay generator, which firstly receives a trigger signal came from the Nd:Glass laser, then after regulating and adding a adjustable delay, sent the trigger signal to the camera. The energy meter was used to monitor the incident pulse laser energy; the energy fluctuation was controlled in $\pm$ 5 %. Figure 3.3 gives a typical high speed camera image of the plasma at t = 3.4 μs, where t is the elapsed time after laser initiation. The evolution history of an ionization front and a shock front can be measured precisely. Temporal and spatial resolutions were, respectively, 30ns and 0.1 mm.

Figure 3.4 portrays the shock front and the ionization frond displacements in argon gas along the laser axis. The displacements of the two fronts coincide with each other during the LSD regime. The point of intersection of these two curves indicates timing of the LSD termination at 0.7 μs. This termination time in air was observed at 0.3 μs in the previous study[6]. Furthermore, the comparison with air and argon is observed on the displacement of the blast wave. In order to consider the ambient gas, a Mach-number, divided by the sound velocity, are also estimated and showed in Fig 3.4. These results indicate that the propagation of LSD depends on the ambient gas species.

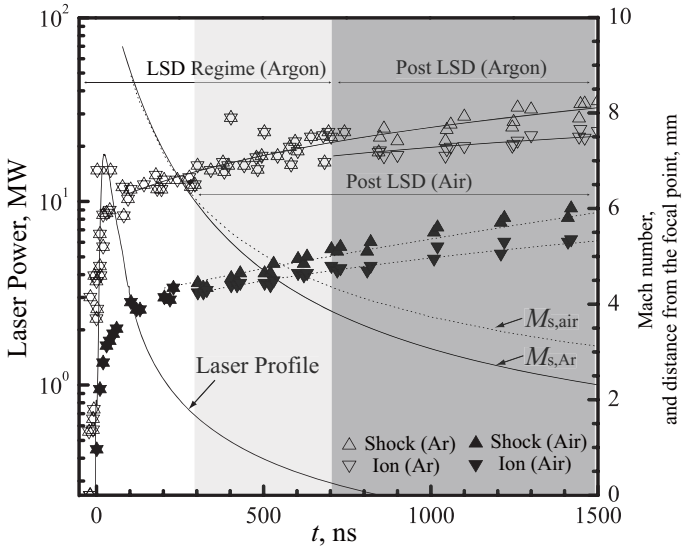

Figure 3.4: Laser pulse shape, displacement of the shock front and the ionization front, and Mach-number as compared with air plasma[6].

Table 3.1: Spectral line data for ArI and NII from NIST[7].

	λ (nm)	A_{ik} (10^7 s^{-1})	E_k (eV)	g_k
Ar I	440.0986	3.04	19.22	6
	454.5052	4.71	19.87	4
	476.4865	6.4	19.87	4
	480.6020	7.80	19.22	6
	484.7810	8.49	19.31	2
	487.9864	8.23	19.68	6
N II	391.900	6.76	23.57	3
	395.585	1.31	22.00	5
	399.500	13.5	22.00	5
	444.703	11.4	23.20	5
	504.510	3.42	20.94	3

3.3 Electron Temperature and Electron Density

To evaluate the number of electron density and the electron temperature, the emission spectroscopy for Ar^+ (see Table 3.1) was used, which are the same as those described in a chapter 1. Figure 2.4 shows a schematic of the emission spectroscopy experiment. We used the eschell spectrometer for these experiments. From the emission spectrum of the laser induced plasma, the information of T_e and n_e can be inferred using, respectively, the Boltzmann plot and the Stark broadening. The temperature and density for air plasma were used for comparison purposes. As a

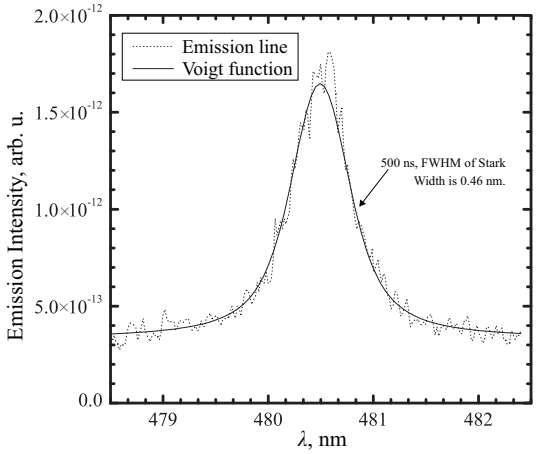

Figure 3.5: Boltzmann plot of ArI at $t = 0.3$ μs.

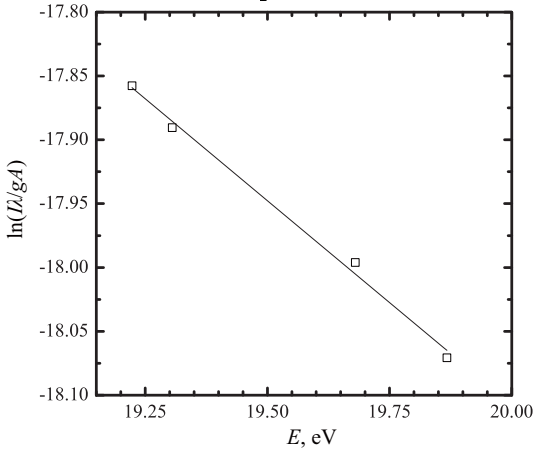

Figure 3.6: Stark Broadening of ArI at $t = 0.3$ μs.

result, in Fig. 3.7, each data plot in argon atmosphere appears to have even high value than in air.

3.4 Radiation Volume

Because of the low angle of laser light channel (2.3 degrees), we shall introduce a sharp cone as a approximation LSD model that is shown in Fig. 3.8. The volume involeved in radiation layer V (m^3) can be expressed as,

$$V = \frac{\pi}{3}\left(\frac{1}{2f}\right)^2 [z^3 - (z - l_a)^3] \approx \frac{\pi z^2 l_a}{4f^2} \tag{3.1}$$

where, f is the focusing number, r stands for the LSD wave-surface radius and z expresses the LSD wave displacement along the laser light channel from the focusing point. The laser absorption layer l_a can be estimated using Eqs. (2.5) and (2.6) that are the equation of inverse bremsstrahlung absorption. Based on

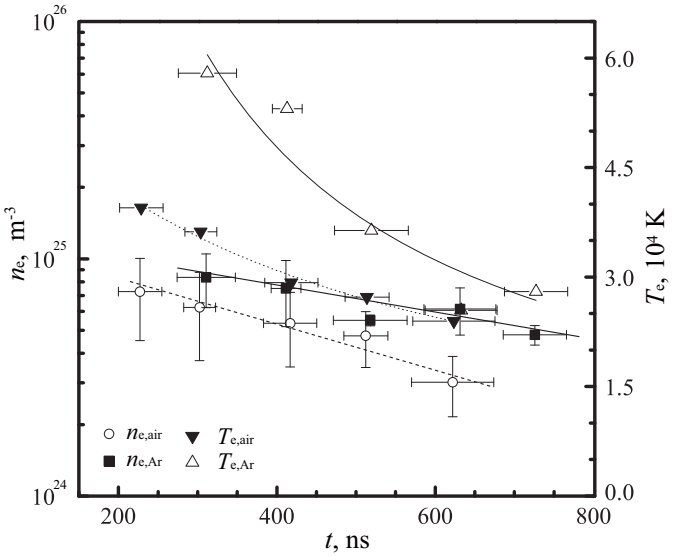

Figure 3.7: Electron temperature and electron density for argon plasma as compared with air plasma.

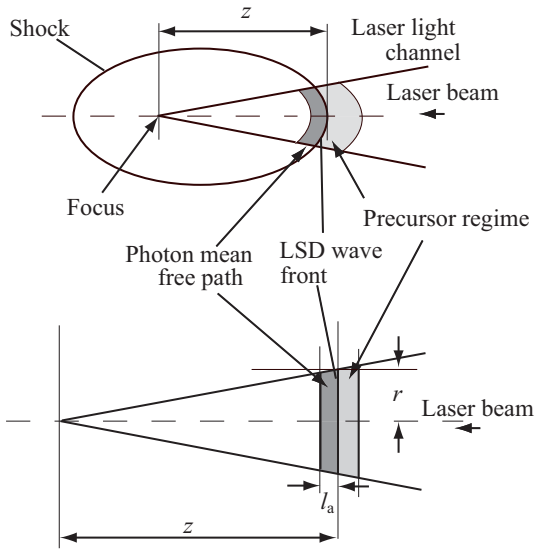

Figure 3.8: Schematic and approximation model for the LSD wave.

Eqs. (2.5) and (2.6), $A(T_e)$ for argon atmosphere can be estimated from the literature[8]. Figure 3.9 shows that the layer of argon plasma is higher than that of air plasma during the LSD regime.

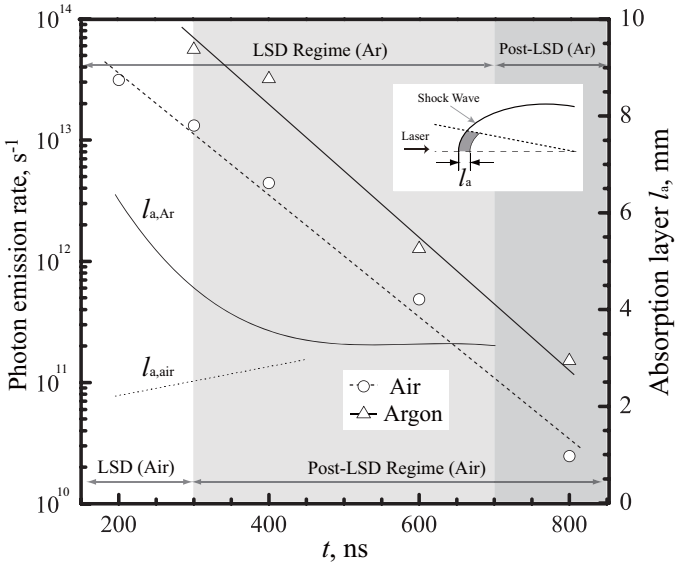

Figure 3.9: Photon emission rate and absorption layer length for air and argon atmosphere.

3.5 Photon Emission Rate

In the laser plasma, UV radiation is induced by the interaction of high energy electron. The bremsstrahlung radiation energy W (W/m^3), which can contribute to single-photon ionization ahead of the shock wave, is expressed as[9]

$$W = \int_{\nu_\mathrm{i}}^{\infty} w(\nu)\mathrm{d}\nu = \int_{\nu_\mathrm{i}}^{\infty} 6.3 \times 10^{-53} \sqrt{\frac{e}{k_\mathrm{B}T_\mathrm{e}}} n_\mathrm{e} n_\mathrm{i} \exp\left(-\frac{h\nu_\mathrm{i}}{k_\mathrm{B}T_\mathrm{e}}\right) \mathrm{d}\nu \tag{3.2}$$

$$S_\mathrm{phi} = \frac{WV}{h\nu_\mathrm{i}} = 6.3 \times 10^{-53} \sqrt{\frac{e}{k_\mathrm{B}T_\mathrm{e}}} n_\mathrm{e} n_\mathrm{i} \frac{k_\mathrm{B}T_\mathrm{e}}{h\nu_\mathrm{i}} \exp\left(-\frac{h\nu_\mathrm{i}}{k_\mathrm{B}T_\mathrm{e}}\right) V \tag{3.3}$$

This formula is derived from the Rutherford scattering. Here, ν_i is the ionization threshold frequency for argon atom, which is related to the wavelength 75.2 nm. n_i, h and k represent the number density of ions, Planck's constant and the Boltzmann 's constant, respectively. It can be seen from Fig. 3.9 that the photon emission rate for argon plasma is higher than that for air plasma. Besides, the argon plasma emitted a single photon in 10^{-9} to 10^{-14} seconds. Comparing these results with those from Fig. 3.4, the photon emission rate is related to the propagation of blast wave and maintenance of LSD. Since the large number of photons sustains the LSD wave during the long period, the LSD duration of argon plasma is longer than that of air plasma.

3.6 Conclusion

To estimate the UV photons emitted from the plasma, we used the emission spectroscopy and the laser-shadow graph to investigate the plasma diagnostics. And

high-purity argon was used as the test gas for comparison with air. As a result, the both of electron temperature and density in the argon laser plasma behind the shock wave were higher than in air plasma. Besides, the argon plasma emitted a single photon in 10^{-9} to 10^{-14} seconds, which was higher value as compared with air plasma. From the comparison of the argon plasma and air plasma, it can be concluded that the LSD in argon gas sustains high dense plasma and generates the photons-contributing photoionization in relatively large number. Thus, the LSD wave in argon gas was sustained longer than that of air.

Bibliography

1) Kantrowitz, A., " Propulsion to Orbit by Ground Based Lasers, Aeronaut. Astronaut. 10, 74 (1972).

2) Myrabo, L.M., Messitt, D.G. and Mead, F. B., " Ground and Flight Tests of a Laser Propelled Vehicle, AIAA Paper, 98-1001 (1998).

3) Mori, K., Komurasaki, K. and Arakawa, Y., " Nozzle Scale Optimum for the Impulse Generation in a Laser Pulsejet, J. Spacecr. Rockets 41, 887 (2004).

4) 嶋村 耕平, 畑井 啓吾, 河村 好一, 福井 章泰, 福田 章雄, 王 彬, 山口 敏和, 小紫 公也, 荒川 義博 : 2 波長マッハツェンダー干渉法を用いたレーザー支持爆轟波構造の解明, 日本航空宇宙学会論文集, 58, 323-329 (2010)

5) Zheleznyak, M. B., Mnatsakanyan, A. K. and Sizykh, S. V.: PHOTOIONIZATION OF NITROGEN AND OXYGEN MIXTURES BY RADIATION FROM A GAS-DISCHARGE, High Temperature 20, 357-362 (1982)

6) B. Wang, K. Komurasaki, T. Yamaguchi, K. Shimamura, and Y. Arakawa, J. Appl. Phys. 108, 124911 (2010).

7) NIST Atomic Spectra Database, http://physics.nist.gov.

8) K. Mori, K. Komurasaki, and Y. Arakawa, J. Appl. Phys. 92, 5663 (2002).

9) John, T.L.: Free-free transitions of atomic and molecular negative-ions in infrared. Mon. Not. R. astr. Soc. 170, 5-6,(1975)

10) 加藤進，高橋栄一，佐々木明，岸本泰明: 放電・雷における原子・分子過程のモデル化，Journal of Plasma and Fusion Research, 84. 477-485 (2008)

Chapter 4

CONCLUSION

From the experimental result, we can conclude that;

- the photon means free path at wavelength of 1,053 nm is longer than at wavelength of 10.6 μm,
- the LSD wave induced using the glass laser is sustained with the highly dense plasma, in comparison with that using the CO_2 laser,
- the argon laser-plasma maintains the high electron temperature and high electron density as compared with air plasma, and
- the argon plasma emitted a single photon 10^{-9} to 10^{-14} seconds, which is higher value as compared with air plasma.

WORKS

Publications

1. 嶋村耕平, 畑井啓吾, 河村好一, 福井章泰, 福田章雄, 王彬, 山口敏和, 小紫公也, 荒川義博, "2 波長マッハツェンダー干渉法を用いたレーザー支持爆轟波構造の解明 " 日本航空宇宙学会論文集, 東京, Vol. 58, No. 682, pp.323-329,(2010).

2. Wang B., Komurasaki K., Yamaguchi T., Shimamura K. and Arakawa Y., " Energy conversion in a Glass-laser-induced blast wave in air " Journal of Applied Physics, USA, Vol.108, 124911 (2010)

3. Shimamura K., Hatai. K., Kawamura. K., Fukui. A., Fukuda. A., Wang. B., Yamaguchi. T., Komurasaki. K. and Arakawa. Y., " Internal Structure of Laser Supported Detonation Waves by Two-Wavelength Mach-Zehnder Interferometer ", Journal of Applied Physics, USA, (to be published).

Conference Papers

1. ○ Shimamura K, Sawahara H, Oda A, Komurasaki K, Arakawa Y," A cost Evaluation for Transport of Solar Power Satellite by Beam Energy Propulsion ", Asian Joint Conference on Propulsion and Power 2010,AJCPP2010-009, Miyazaki City, JPN, Mar., 2010

2. ○ Wang B., Han T., Shimamura K., Yamaguchi T., Komurasaki K. and Arakawa Y.," Study of laser propulsion efficiency from solid state laser to shock wave energy in reduced ambient pressure ", 61 st International Astronautical Congress, IAC-10.C4.8.3, Pragure, Czech Republic, 2010,

3. ○ Shimamura K, Wang B., Komurasaki K. and Arakawa Y," Laser Supported Detonation in Argon gas "49th AIAA Aerospace Sciences Meeting and Exhibit, AIAA-2011-1139, Orlando, Florida, USA, January, 2011

4. ○ Shimamura K, Michigami K., Wang B., Yamaguchi T., Komurasaki K. and Arakawa Y,"Laser Wavelength Dependency of Laser Supported Detonation", 7th International Symposium on Beam Energy Propulsion, Germany, April, 2011.

5. ○ Shimamura K, Michigami K., Wang B., Komurasaki K. and Arakawa Y,"Photoionization in the Precursor of Laser Supported Detonation by Ul-

traviolet Radiation", 7th International Symposium on Beam Energy Propulsion, Germany, April, 2011.

Conference in Japan

1. ○嶋村耕平, 澤原弘憲, 小田章徳, 小紫公也, 荒川義博,“ ビームエネルギー推進による SPS 輸送コスト評価 ”, 第 12 回宇宙太陽発電システムシンポジウム,pp46-50, 京都,2009 年 11 月.

2. ○嶋村耕平, 澤原弘憲, 小田章徳, 小紫公也, 荒川義博,“ ビームエネルギー推進を用いた宇宙太陽光発電の輸送 ”平成 21 年度宇宙輸送シンポジウム,STEP2009-49, 相模原,2010 年 1 月.

3. ○ Wang Bin, 嶋村耕平, 山口敏和, 小紫公也, 荒川義博,“ Experimental Investigation on the Shock Wave Generated by a Solid Laser Induced Plasma in Air ”, 平成 21 年度衝撃波シンポジウム,19-C-3-1, 大宮,2010 年 3 月.

4. ○ Wang Bin, 嶋村耕平, 山口敏和, 小紫公也, 荒川義博,“ ガラスレーザーによるレーザーの誘起プラズマの生成と衝撃波の伝播 ”日本航空宇宙学会第 41 期年会講演会,C28, 本郷,2010 年 4 月

5. ○福成雅史, 嶋村耕平, 道上啓亮, 葛山浩, 小紫公也, 荒川義博, “ マイクロ波ロケットによる単段式打ち上げの検討 ”第 54 回宇宙科学技術連合講演会，静岡，2010 年 11 月.

6. ○道上啓亮, 嶋村耕平, 王彬, 山口敏和, 小紫公也, 荒川義博, ”レーザー支持爆轟波の伝播構造における気体種依性 ”レーザー学会学術講演会第 31 回年次大会,, 調布，2011 年 1 月.

7. ○道上啓亮, 嶋村耕平, 王彬, 班太郎, 小紫公也, 荒川義博,” レーザー支持爆轟波性能の f 値及び気体種依存”, 第 51 回航空原動機宇宙推進講演会,JSASS-2011-002, 広島市,2011 年 3 月.

8. ○嶋村耕平, 道上啓亮，王彬, 小紫公也, 荒川義博，”レーザー支持爆轟波前方における光電離構造”, 平成 22 年度衝撃波シンポジウム，相模原，2011 年 3 月.